

# Quantum measurement fitting

P.T. Eendebak<sup>1</sup>

<sup>1</sup>QuTech and Netherlands Organization for Applied Scientific Research (TNO), Stieltjesweg 1, 2628 CK Delft, Netherlands

March 5, 2025

## Abstract

Quantum measurements are not deterministic. For this reason quantum measurements are repeated for a number of shots on identically prepared systems. The uncertainty in each measurement depends on the number of shots and the expected outcome of the measurement. This information can be used to improve the fitting of models to quantum measurements.

In this paper we analyse ordinary-least squares, weighted least squares and maximum-likelihood estimation. We show that using the information on the quantum measurement uncertainty can lead to improved estimation of system parameters. We also introduce the concept of model violation and demonstrate it can be a valuable tool to analyze model assumptions and performance of quantum systems.

## 1 Introduction

Measurements on quantum systems often consist of a system initialization, manipulation and readout. This cycle is repeated multiple times to obtain a measurement histogram. For calibrations of quantum systems often variations of the manipulation stage are measured, resulting in 1-dimensional datasets. An example is a Rabi oscillation which is used to calibrate the duration of an X90 gate [7, section 4.3].

For a single-qubit quantum system in the state  $\alpha|0\rangle + \beta|1\rangle$  the probability of finding the system in state  $|1\rangle$  upon measurement is  $p = |\beta|^2$ . When measuring identically prepared quantum states for  $N$  times the number of counts  $k$  of the  $|1\rangle$  state is a value between 0 and  $N$  (inclusive), distributed according to the binomial distribution which has probability mass function

$$B(k, N, p) = \binom{N}{k} p^k (1-p)^{N-k}. \quad (1)$$

The mean and variance of this distribution are given by  $\mu = p$  and  $\sigma^2 = p(1-p)/N$ , respectively.

To obtain information about operational parameters of quantum systems we often perform calibration experiments where we fit models with parameters to measured data points. Examples are a  $T_1$  measurement (fitting an exponential decay), a  $T_2^*$  measurement (fitting a damped sine wave) or a qubit spectroscopy measurement (fitting a Rabi model).

In this paper we compare several methods to fit the models to the data and analyse the properties of the estimated parameters. In particular we pay attention to the bias and variance of the estimated parameters.

## 2 Methods

In this work we consider a model  $F(x, \theta)$  that depends on a number of parameters  $\theta = (\theta_0, \dots, \theta_k)$  and independent data variable  $x$ . An example is an exponential decay  $F(x, \theta) = \theta_0 \exp(-\theta_1 x)$  or a sine  $F(x, \theta) = \theta_0 + \theta_1 \sin(\theta_2 x + \theta_3)$ . In typical experiments we measure  $m$  datapoints  $(x_j, y_j)$ ,  $1 \leq j \leq m$  with  $y_j = k_j/N$ , with  $k_j$  the number of times the  $|1\rangle$  state was measured.

## 2.1 Fitting methods

Most curve fitting methods depend on a cost function and a non-linear optimizer [4]. In this section we focus on the cost function. In ordinary least squares (OLS) [17] one optimizes the cost function

$$J_{\text{OLS}}(\theta) = \sum_{j=1}^m |F(x_j, \theta) - y_j|^2. \quad (2)$$

The OLS estimate for the unknown parameters is

$$\hat{\theta}_{\text{OLS}} = \arg \min_{\theta} J_{\text{OLS}}(\theta). \quad (3)$$

To find the estimate usually an initial guess is provided and a non-linear optimization method is applied to the cost function.

Alternative fitting methods are weighted least squares (WLS) and maximum-likelihood estimation (MLE). The WLS cost function is

$$J_{\text{WLS}}(\theta) = \sum_{j=1}^m w_j |F(x_j, \theta) - y_j|^2 \quad (4)$$

for a suitable choice of weights  $w_j$ . The choice of weights typically depends on the application. According to the Gauss-Markov theorem [16] using weights  $w_j = 1/\sigma_j^2$ , with  $\sigma_j^2$  the variance of the  $j$ th measured datapoint results in the best linear unbiased estimator (BLUE estimator).

The MLE cost function is defined as the negative log-likelihood

$$\begin{aligned} J_{\text{MLE}}(\theta) = -\mathcal{L}(\theta) &= -\log \left( \prod_{j=1}^m B(k_j, N, F(x_j, \theta)) \right) \\ &= -\sum_{j=1}^m \log \left( \binom{N}{k_j} F(x_j, \theta)^{k_j} (1 - F(x_j, \theta))^{N-k_j} \right) \\ &= \text{constant} - N \sum_{j=1}^m (y_j \log(F(x_j, \theta)) + (1 - y_j) \log(1 - F(x_j, \theta))), \end{aligned} \quad (5)$$

with  $y_j$  the measured fraction for the  $j$ th datapoint. The maximum-likelihood estimation optimizes the parameters to maximize the probability of observing the measured data.

The WLS method requires a choice of the weights  $w_j$ . A natural choice is to take  $w_j = 1/\sigma_j^2$  with  $\sigma_j^2$  the variance of the probability for the  $j$ th datapoint. However, we do not know the real value of the probability a priori, so we need to make a suitable estimate. This process is called bootstrapping [15]. Both the WLS and the MLE methods require regularization. The regularization is required to avoid the singularities in the cost functions for probabilities near 0 and 1. Another variation on the above methods is iteratively reweighted least squares (IRLS). In this method the WLS cost function is used, but weights are adapted on each iteration according to the current estimate of the parameters.

### 2.1.1 Initial estimates and optimization

The optimization of a cost function is performed by starting with an initial guess of the parameters. In this paper we assume that we have a procedure available to produce a reasonable initial guess (either from the data or provided by the user). Starting with the initial guess the parameters of the model are optimized using a local optimization procedure such as gradient descent or Levenberg-Marquardt [8].

All results in this paper have been obtained with LMfit-py [9] using the `least-squares` method. We have not observed different results with other optimizers. The optimization with the non-OLS methods has been performed with initial parameters set to the output of the OLS fit.

### 2.1.2 Bootstrapping

From the observed data  $y$  we want to obtain an estimate for the true probabilities  $p_j$  and the variance  $\sigma_j^2$  for each datapoint. To obtain an estimate for the values of  $p_j$  and the variance  $\sigma_j^2$  we have several options

**Baseline** We take  $p_j = y_j$  and estimate the variance using the binomial  $\sigma_j^2 = y_j(1 - y_j)/N$ . The variance is thus estimated from the measured datapoints.

**Jeffreys prior** We use the measured datapoints  $y_j$  to update a prior distribution to a posterior distribution. A reasonable choice for the prior distribution is Jeffreys prior with equal probability for the  $|0\rangle$  and  $|1\rangle$  states (this choice for the prior is used in Qiskit [1]). The observation of the datapoint  $y_j$  then leads to estimates

$$p_j = \frac{Ny_j + 1/2}{N + 1}, \quad \sigma_j^2 = \frac{p_j(1 - p_j)}{N + 2}. \quad (6)$$

**Wilson** From the estimates  $p_j$  we determine the Wilson score interval [18] for  $z = 1$ . We estimate the variance as the centre of the score interval.

**Prediction** We use the OLS estimates of the model parameters  $\theta$  to predict values  $\tilde{y}_j$  and then use  $p_j = y_j$ ,  $\sigma_j^2 = \tilde{y}_j(1 - \tilde{y}_j)/N$ . We can also use  $p_j = \tilde{y}_j$  in combination with one of the methods described above. This creates more balanced estimates for the variance and avoids using small variances for datapoints that are close to 0 or 1 due to the random component in the measurements.

More variations are possible, but with these options we have introduced the main concepts used in bootstrapping.

### 2.1.3 Regularization

Some of the bootstrapping methods described above already introduce some regularization, but some others do not. Regularization is applied to either the probabilities  $p_j$  or the variances  $\sigma_j^2$  or both. The regularization has several goals:

- Prevent errors in the optimization at the singularities  $p = 0$  and  $p = 1$ .
- Prevent errors when a predicted probability is outside the  $[0, 1]$  range. That can happen for certain models when the parameters are automatically varied by the optimizer. But also error mitigation techniques like readout error mitigation can introduce pseudo-probabilities with negative values.
- Without regularization the optimizers tend to converge to local minima more often.

A good regularization should address the issues mentioned above, and at the same time

- Avoid bias in the fitting procedure
- The regularization should be differentiable (which improves performance of local optimizers)

All regularization methods considered have a parameter  $\epsilon$  that describes the regularization strength. Typically, the value is regularized for  $p_j < \epsilon$ , while values  $p_j > \epsilon$  are hardly affected by the regularization (and similar for  $p_j$  near 1). We use the following regularized probability on our experiments:

$$r(p, \epsilon) = \begin{cases} \epsilon/2 & \text{if } p < 0 \\ \epsilon/2 + p^2/(2\epsilon) & \text{if } 0 \leq p \leq \epsilon \\ p & \text{if } \epsilon \leq p \leq 1 - \epsilon \\ 1 - (\epsilon/2 + (1 - p)^2/(2\epsilon)) & \text{if } 1 - \epsilon \leq p \leq 1 \\ 1 - \epsilon/2 & \text{if } p > 1 \end{cases} \quad (7)$$

For the MLE estimation we also have a regularized log function  $\log_r$ . The regularized log is a second order Taylor expansion at  $\epsilon$  for small values [10, section 4.3].

$$\log_r(x, \epsilon) = \begin{cases} \log(\epsilon) + (x - \epsilon)/\epsilon - (x - \epsilon)^2/(2\epsilon^2) & \text{if } x < \epsilon \\ \log(x) & \text{if } x > \epsilon \end{cases} \quad (8)$$

In contrast to [10, section 4.3] we have models that can predict datapoints outside the  $[0, 1]$  interval. For MLE the regularization with the log probability is not enough to avoid predictions outside  $[0, 1]$ . The reason is that

the binomial probability density function for  $y \approx 1$  is zero almost everywhere, rises sharply to a maximum at  $p = 1$  and is zero for  $p > 1$ . The regularization results in a term

$$y \log_r(p) + (1 - y) \log_r(1 - p) \approx \log_r(p). \quad (9)$$

The likelihood is maximal in the interval  $[0, 1]$  for  $p = 1$ . But values  $p > 1$  are rewarded, so we need a penalty term. The penalty term should be high and sharp at the  $p = 0$  and  $p = 1$  boundary. An alternative is using  $\log(r(p))$ . This does not result in a strong penalty for  $p$  outside  $[0, 1]$ , but at least the likelihood for  $p \gg 1$  is not rewarded. In this paper we use the soft penalty term

$$P_{\text{soft}}(p) = (\max(p, 1) - 1 + \min(p, 0))^2 / \epsilon^3. \quad (10)$$

An alternative is a hard penalty

$$P_{\text{hard}}(p) = \begin{cases} 0 & \text{if } p \in [0, 1] \\ L & \text{otherwise} \end{cases}, \quad (11)$$

for  $L$  a large number, e.g.  $L = 1e100$ . The penalty for the maximum likelihood-estimation fitting is the sum of the penalties for all the probability predictions. In appendix A we show results of MLE fitting without a penalty, the soft penalty from equation 10 and the hard penalty from equation 11.

Another view of regularization is that it adds prior information [2] to our problem.

## 2.2 Evaluation criteria

In section 3 we will analyze the performance of the methods described above. We will do this by applying the fitting methods to simulated data. For every simulation we perform, the fitted parameters should ideally be close to the parameters used in the simulation. However, due to the randomness in the generation of the data points, it is not possible for the fitting to always match the ground truth parameters. For every simulation  $s$  we obtain an estimate of the parameters  $\hat{\theta}_s$ . For every method we consider the following properties of the estimator:

$$\text{bias} = (\sum_s \hat{\theta}_s - \theta) / S, \quad (12)$$

$$\text{variance} = \sum_s |\hat{\theta}_s - \theta|^2 / S, \quad (13)$$

$$\text{likelihood} = (1/S) \sum_s \log \mathcal{L}(\hat{\theta}_s), \quad (14)$$

with the summation  $s$  over the different simulations and  $S$  the the number of simulations performed.

From our fitting procedure we want to have a small bias, low variance and high likelihood. These three properties cannot always be optimized simulatenously. In particular there can be a trade-off [14] between the bias and the variance of an estimator. In this work we present results on the bias and variance of the estimators. The likelihood of the estimate, and in particular whether the estimate is the MLE estimate, is considered less important.

## 2.3 Model violation

A measure of the deviation of the measured data to the model predictions is the  $\chi^2$  value. When normalized using the number of degrees of freedom  $d = m - k$ , we have the model violation  $N_\sigma$ .

$$\chi^2 = \sum_j \frac{(y_j - \tilde{y}_j)^2}{\sigma_j^2} = N \sum_{j=1}^m \frac{(y_j - \tilde{y}_j)^2}{\tilde{y}_j(1 - \tilde{y}_j)} \quad (15)$$

$$N_\sigma = \frac{\chi^2 - d}{\sqrt{2d}} \quad (16)$$

The model violation in the context of gate set tomography is described in [10, section 4.3]. For a sufficient amount of data points  $m$  the  $\chi^2$  value is distributed as a  $\chi^2$ -distribution with  $d$  degrees of freedom. The model violation  $N_\sigma$  is then normally distributed and large values of  $N_\sigma$  indicate the measured data cannot be explained by the model and fitted parameters. Any outliers in the data will result in a high model violation. There are techniques to make the fitting robust against the outliers (e.g. robust cost functions [6, section A6.8], RANSAC [3]), but they are not in the scope of this work.

### 3 Results

In this section we compare the different fitting methods. We analyse OLS, WLS with different choices for the weights, and MLE. To obtain weights for the WLS we use the bootstrapping methods described in section 2.1.2.

We generate results by selecting a model  $F$ , simulation parameters  $\theta$ , independent data points  $x$  and a number of shots  $N$ . For a large number of iterations we generate datapoints according to our model, perform fitting of the parameters using one of the methods describing above and compare the fitted parameters  $\hat{\theta}$  with the simulation parameters  $\theta$ .

The main example we use is a sine model

$$F(x, \theta) = A \sin(2\pi f x + \phi) + \text{offset}, \quad (17)$$

with parameters  $\theta = (A, f, \phi, \text{offset}) = (0.48, 1, 1, .5)$ . The independent datapoints  $x$  have been chosen to be 23 linearly spaced datapoints in the  $[0, 4]$  interval. The model with a set of simulated datapoints is shown in figure 1.

The number of shots we focus on is either a small number of shots  $N \sim 60$  or a moderate number of shots  $N \sim 1000$  (in quantum experiments on hardware 100 to a 1000 shots is a typical number). For either a high number of datapoints or a high number of shots asymptotic results guarantee that all the estimators are unbiased, have minimum variance and are asymptotically normal [5]. The regularizations are performed with parameter  $\epsilon = 0.05/N$ , with  $N$  the number of shots from the experiment.

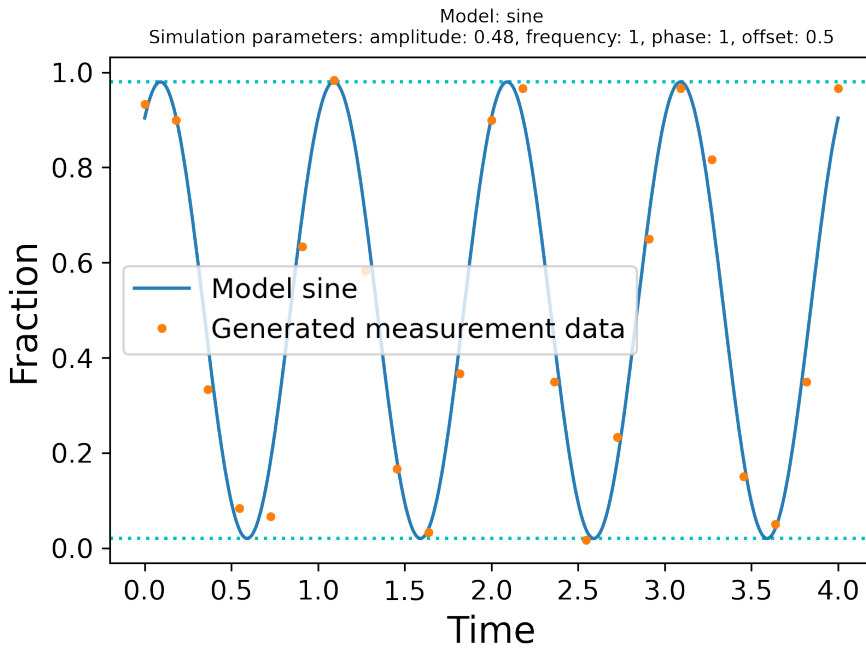


Figure 1: Model and typical measurement data for `sine`.

**Bias and variance** In figure 2 we show the distribution of the estimated `amplitude` parameter for the sine model. The ordinary least-squares method has an estimator with small bias and a variation of about 0.5% in the amplitude.

The weighted least-squares based on the baseline bootstrapping performs poorly. The reason is that datapoints with probability near 0 and 1 can generate measured values very close to 0 or 1 leading to extreme values of the weights. We therefore recommend not to use this approach.

The WLS method with Jeffreys priors has a bias in the amplitude. The reason for this bias is that instead of fitting to the measurement datapoints  $y_j$ , we fit to datapoints  $(y_j + 0.5)/(N + 1)$  (formula 6) which are always closer to 0.5 than the original datapoints  $y_j$ . In the simulation a low number of shots  $N = 60$  has been used, leading to a reduction of the amplitude of datapoints by a factor of 1.6%. This is reflected in a bias of the estimated amplitude.

Model sine, parameter amplitude, N 23, number of shots 60,  
simulation parameters 'amplitude': 0.48, 'frequency': 1.0, 'phase': 1, 'offset': 0.5

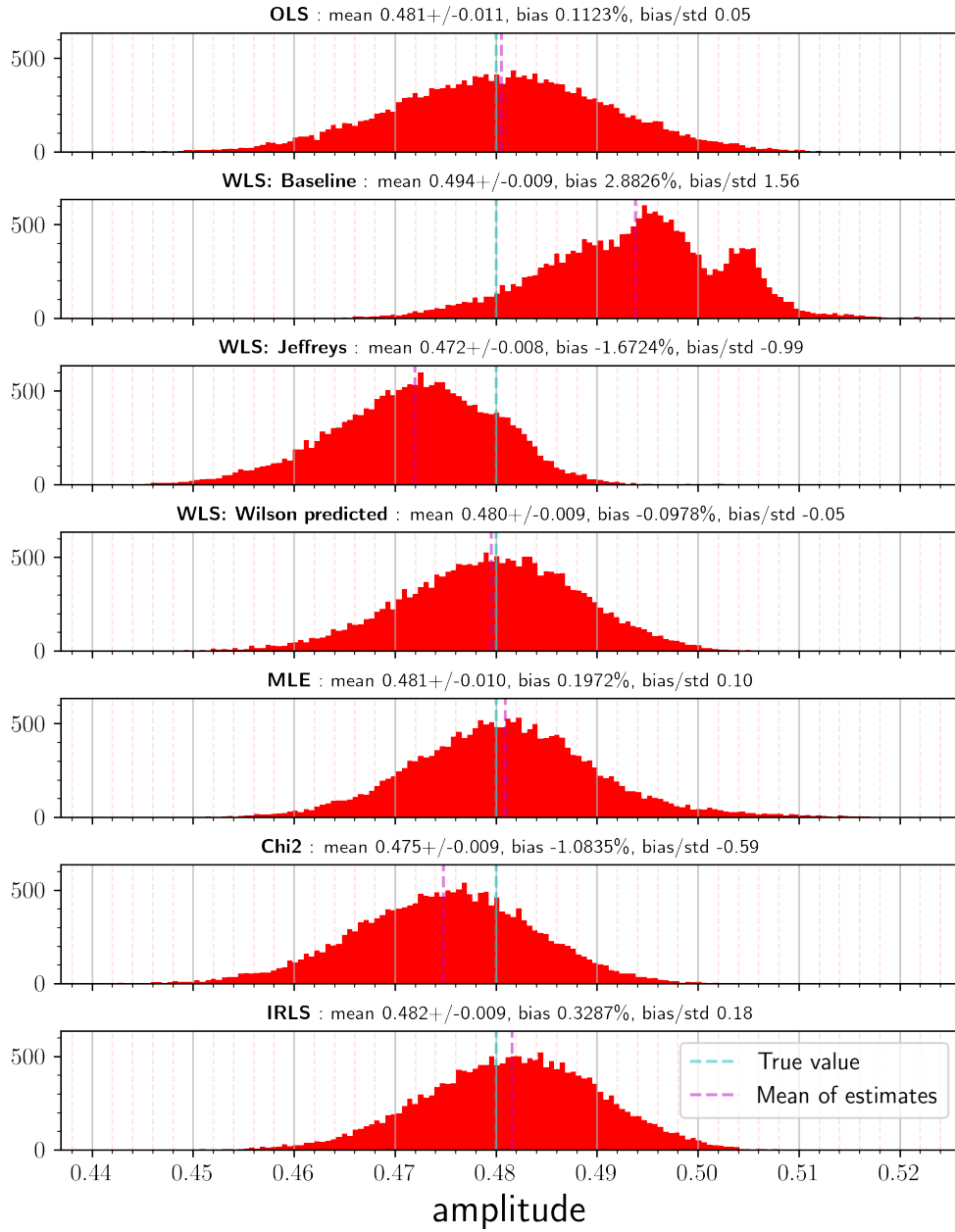


Figure 2: Distribution of the **amplitude** parameter for a **sine** model. For each method we show the mean and standard deviation of estimated parameter  $\hat{\theta}$ , the bias with respect to the simulation parameter and the ratio of the bias and the variation.

Model sine, parameter frequency, N 23, number of shots 60,  
simulation parameters 'amplitude': 0.48, 'frequency': 1.0, 'phase': 1, 'offset': 0.5

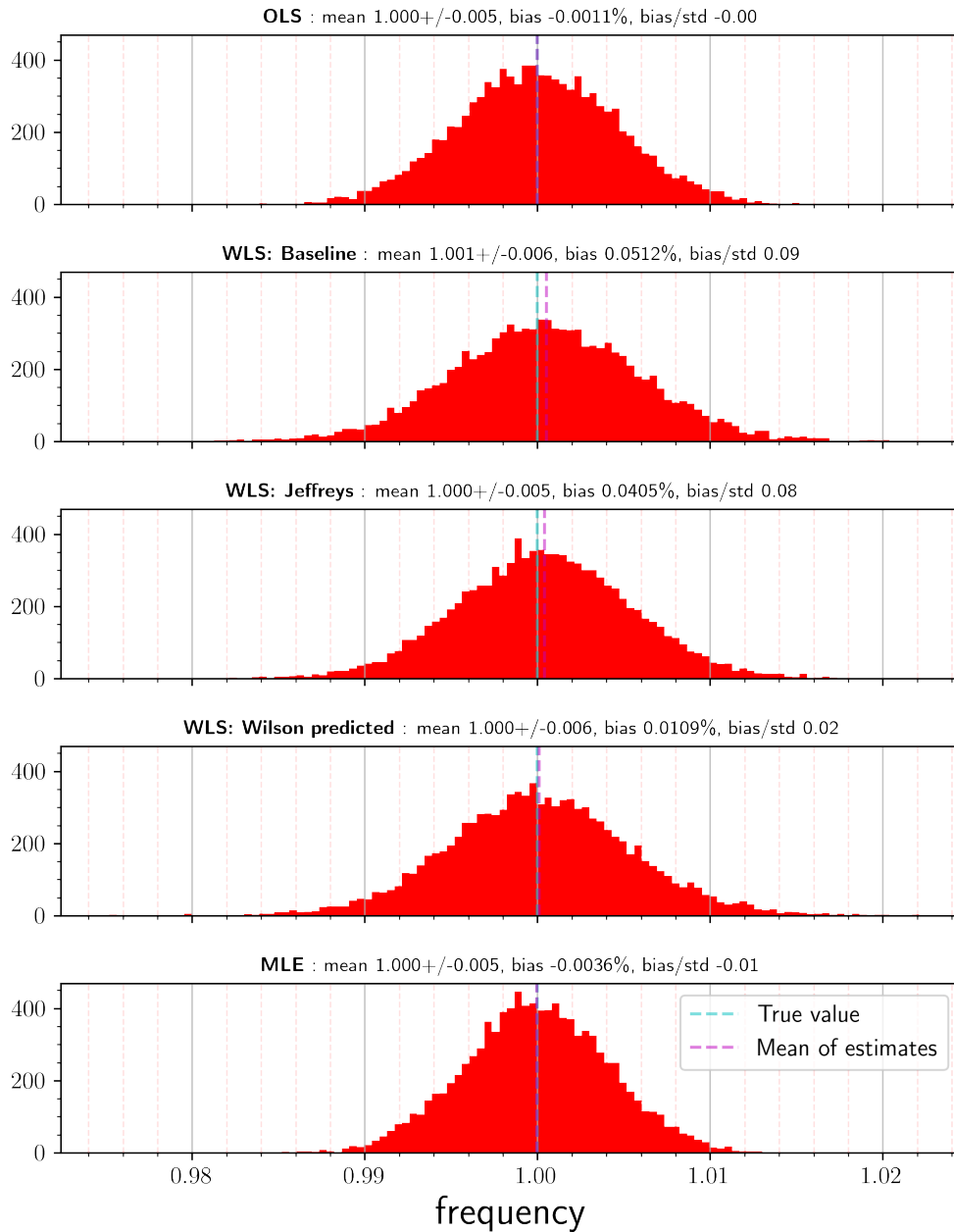


Figure 3: Distribution of the frequency parameter for a sine model. For each method we show the mean and standard deviation of estimated parameter  $\hat{\theta}$ , the bias with respect to the simulation parameter and the ratio of the bias and the variation.

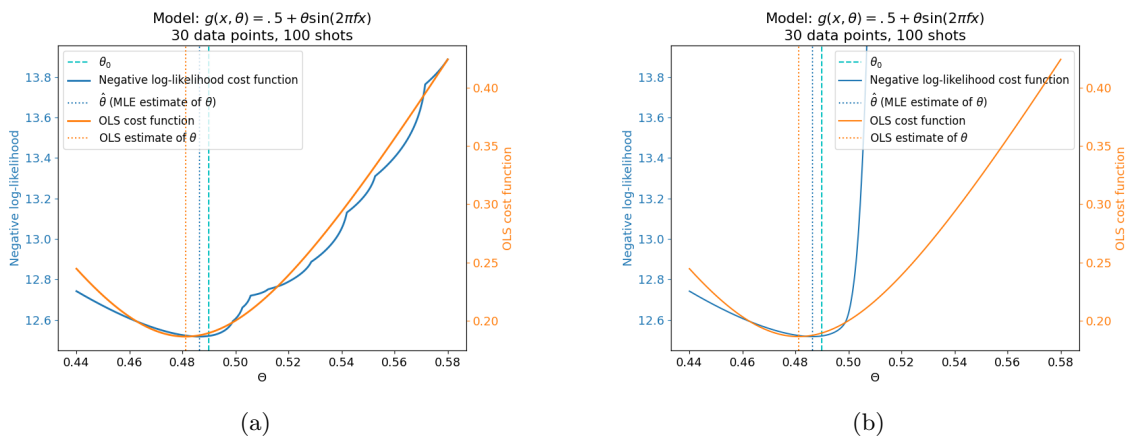


Figure 4: Cost function of a sine model with the OLS cost function and a MLE cost function (negative regularized log-likelihood). The regularization in a) is with a regularized probability  $p_r = \text{clip}(p, \epsilon, 1 - \epsilon)$  and in b) with the regularized log function  $\log_r$  (equation 8).

Both the WLS with predicted variance and the maximum likelihood-estimation perform better than the ordinary least-squares, but the improvement is only modest. The variance is smaller and there is a smaller tail in the distribution. The  $\chi^2$  based fitter (using  $\chi^2$  as a proxy for the log-likelihood) is biased. This was already noted in [11, Appendix E], in the context of gate set tomography. The iteratively reweighted least-squares (IRLS) has a bias towards a lower amplitude. The reason for this is that higher amplitudes result in higher weights and therefore in general higher values of the cost function. This favors the method to avoid high amplitudes.

In a similar way we find the estimate of the frequency parameter is an unbiased estimate for all the methods, with standard deviation of about 0.5% (figure 3). To put this number into perspective: to obtain a single-qubit fidelity on an  $X$  gate of 99.9% one needs an accuracy in the frequency estimate of 2% [13, Table I].

**Importance of regularization and bootstrapping** Without suitable regularization the cost functions can have local minima or flat plateaus, leading to non-optimal solutions or slow convergence. An example of the regularization with a non-differentiable method is shown in figure 4. The effect of the regularization for the exponential model is analysed in further detail in appendix A.1.

**Correlations between parameter estimates** When making a scatter plot between two of the parameters we can see correlations between the parameters.

For example in figure 5 one can see a sharp line of MLE estimates with hardly any estimates above. The reason for this is the following: if the sum of the **offset** and **amplitude** is larger than one, our model predicts a measured fraction outside the valid probability range  $[0, 1]$ . The OLS method allows these terms (with the usual quadratic cost), but for the MLE estimator this results in a strong penalty term (determined by the regularization).

**Number of samples and data points** The variance in the estimated parameters depends on the number of shots and the number of datapoints. More samples or more data points lead to better estimates. However, for practical reasons it is desirable to keep both small.

In figure 6 we show how the mean and variance of the estimate depend on the number of shots. For a large number of shots the three different methods have estimators with the same mean and similar variance. The WLS method performs best overall in terms of the variance.

The MLE estimation is efficient in the limit of a large number of samples. This is shown in figure 7. For typical quantum experiments the number of data points is less than a hundred, so we are in the region where we transition from outliers (due to a small number of samples) and an efficient estimator (in the large number of samples limit).

**Correlation between estimates of different methods** The values of the fitted parameters with respect to the true parameter values depend on the data points. There is a strong correlation between the different methods (figures 8 and 9). For a given model the MLE estimates of a parameter can be both higher and lower than the OLS estimates. But in general a high estimate for OLS implies also a high estimate for WLS or MLE.

**Model violation as a diagnostic tool** The model violation  $N_\sigma$  can be used as a tool to identify problems with quantum systems or model assumptions. We give two examples from actual quantum measurements.



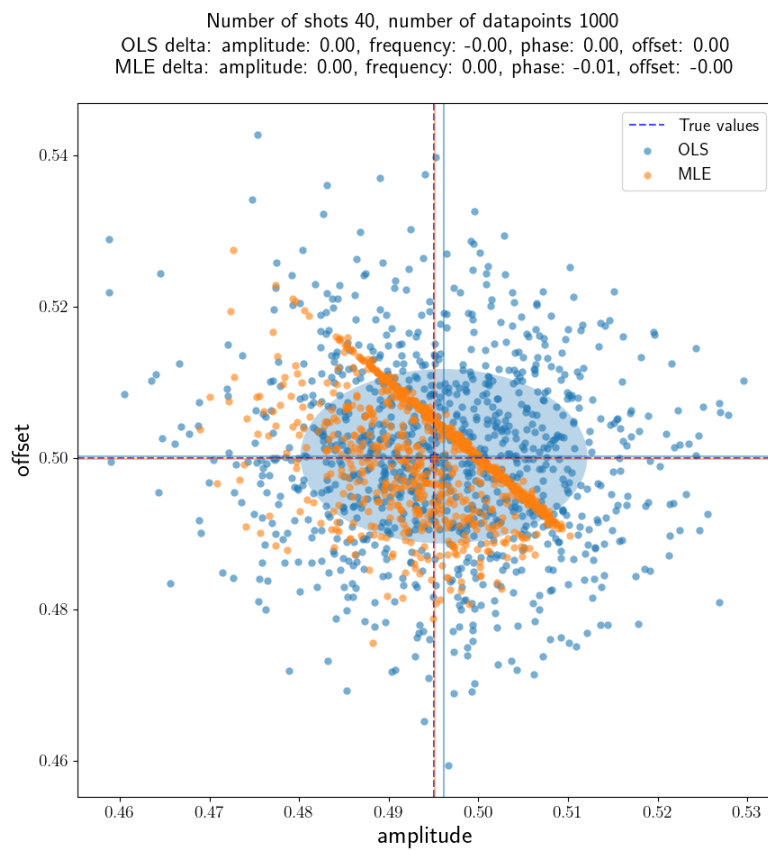


Figure 5: Scatter plot of OLS and MLE fits. The MLE has a penalty cost for data points outside the region of datapoints in the probability region  $[0, 1]$ . The result is a cluster of datapoints along the line  $\text{offset} + \text{amplitude} = 1$ .

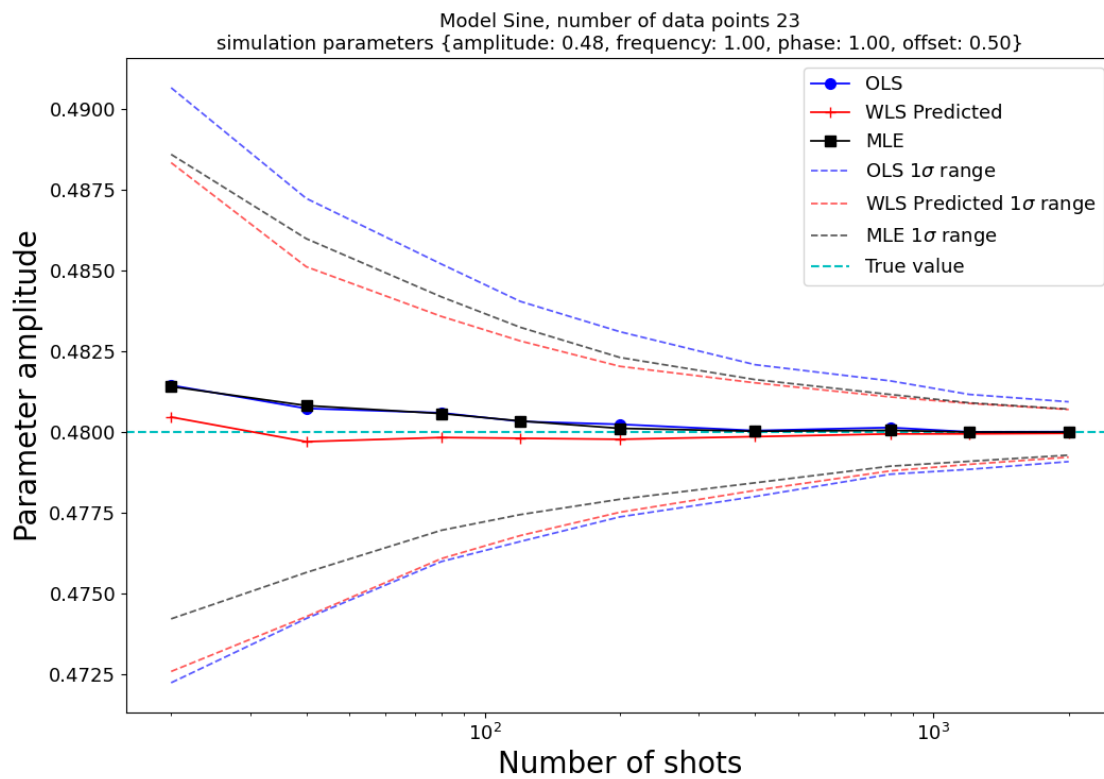
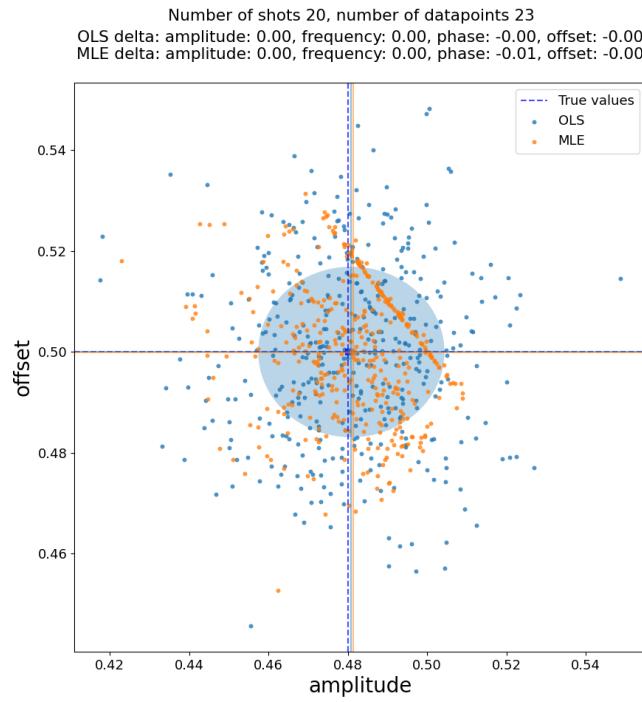
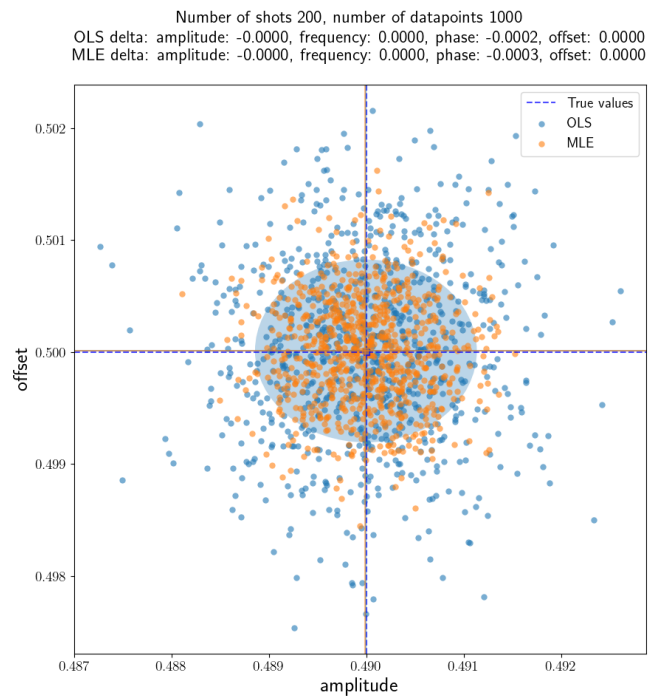


Figure 6: Dependence of the fitting accuracy on the number of datapoints. For different fitting methods we have simulated 8000 experiments and calculated the mean and standard deviation of the fitted parameters. As expected the accuracy roughly scales as one over the square root of the number of shots.



(a) Small number of shots and small number of samples. The MLE fitting shows fewer outliers with respect to the value of the true parameters. Also the boundary of the valid probability predictions is visible.



(b) Large number of samples. The MLE estimates show no outliers, and have a smaller variance than the OLS estimates.

Figure 7: Fitting a sine model with OLS (red) and MLE (blue). The fitted **amplitude** and **offset** are shown in a scatter plot.

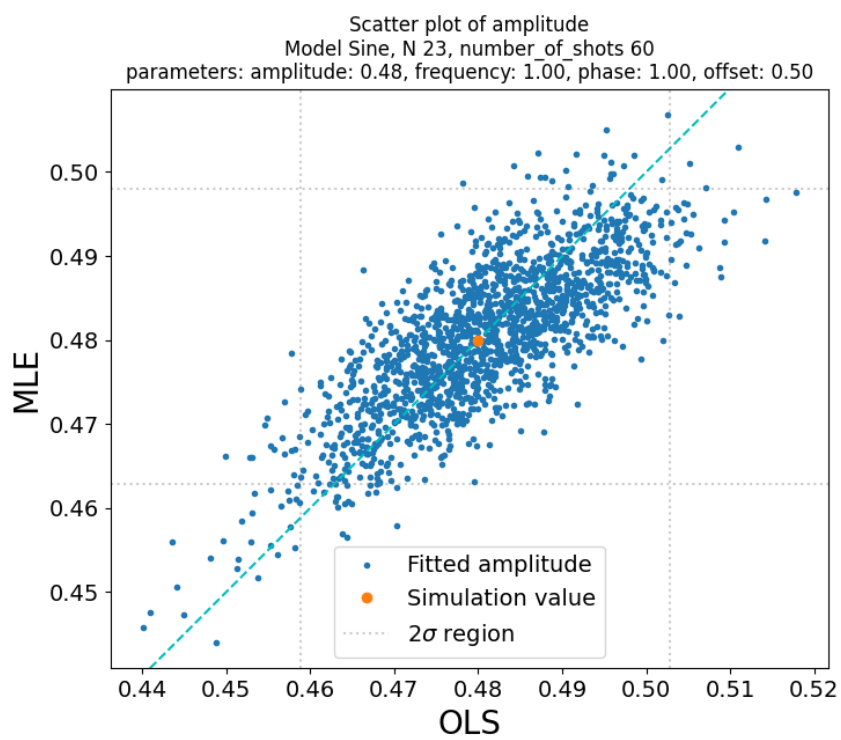


Figure 8: Scatter plot of the `amplitude` parameter for OLS and MLE. The difference between the OLS and MLE estimate of `amplitude` has zero mean and standard deviation of 0.0068.

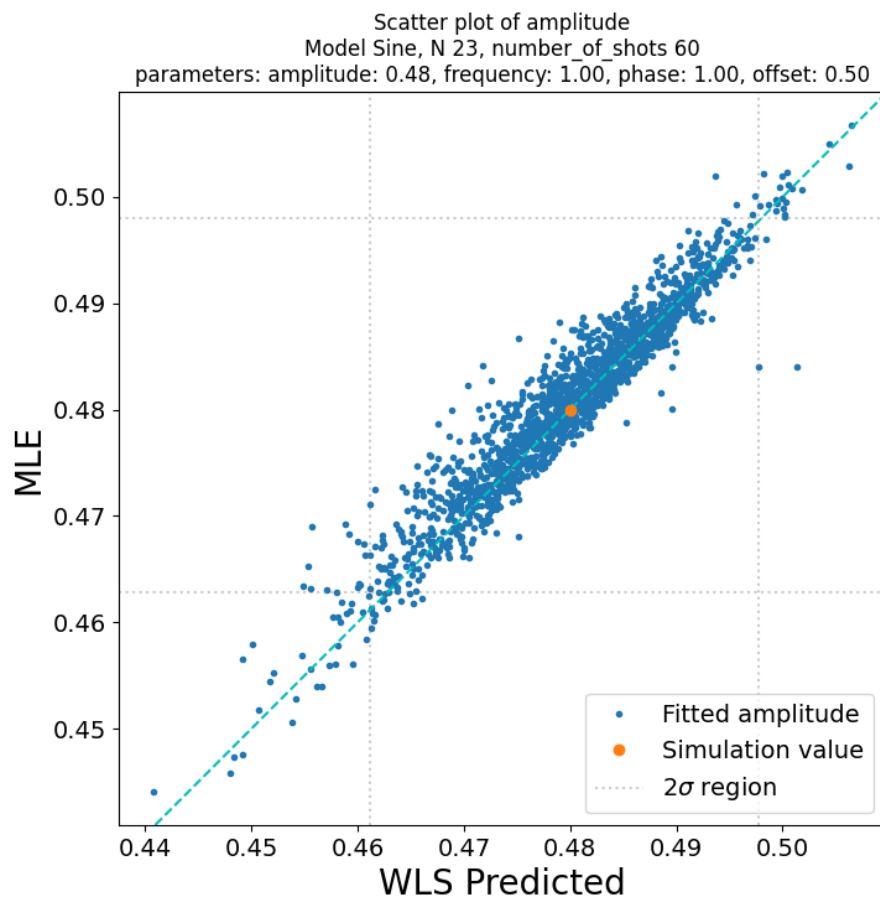


Figure 9: The amplitude is sensitive to regularization of the data points or the variance. Most of the time there is a very strong correlation between the results. But there are cases where there is a large difference due to different local minima

The first example is data from the calibration sequence of a 6-qubit device [12, Figure 4c] where a fit is performed in a spectroscopy experiment. The model fitted is

$$F(x, \theta) = A + B \frac{\Omega^2}{\Omega^2 + (x - \omega_0)^2} \sin^2(\sqrt{\Omega^2 + (x - \omega_0)^2} t / 2),$$

with parameters  $\theta = (A, B, \Omega, \omega_0)$  and  $t = \pi$  the rotation angle. The parameters are the offset  $A$ , visibility  $B$ , Rabi frequency  $\Omega$  and the applied microwave frequency  $\omega_0$ . In the spectroscopy experiment from [12] a standard fit with  $t = \pi$  is performed. The measured data with the fitted model is shown in figure 10. The fitted data looks good at first sight, but the model violation (for  $N = 1000$ )  $N_\sigma = 2.55$  is on the high side. In particular the data and model seem to deviate at the side-lobes. In this case it turns out that the experiment was performed with a small over-rotation of the pulse. If we repeat the model fitting, but also allow the angle parameter  $t$  to vary, we find a model violation of  $N_\sigma = 0.65$  and a rotation angle of  $1.05\pi$ .

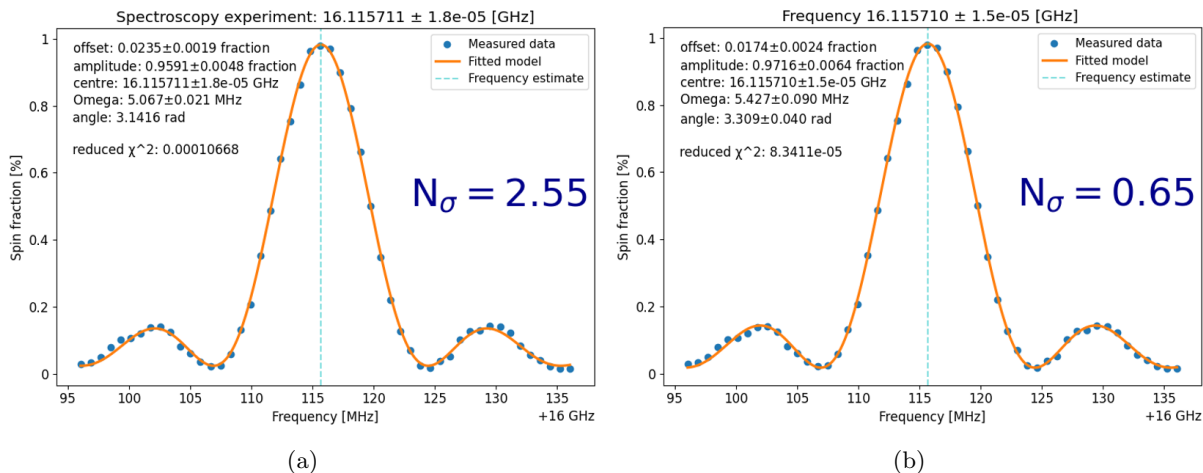


Figure 10: Model violation for a spectroscopy experiment. In (b) the rotation angle  $t$  is estimated to be  $1.05\pi$  radians.

The second example is a series of  $T_2^*$  measurements on the Starmon-5 device of Quantum Inspire [7]. Over a period of a few weeks measurements of the  $T_2^*$  coherence time have been measured for all the 5 qubits. A boxplot with the data is in figure 11. There is variation of the  $T_2^*$  between the qubits, but also for a single qubit there is quite some variation of the value with some strong outliers. In figure 12 the model violation has been plotted for the different qubits versus the time. Qubit number 3 and 4 show poor fits. We picked one of the outlier points with  $\chi_r^2 = 914$  and  $T_2^* = 15.0$  us. The data for this measurement is shown in figure 13.

## 4 Discussion

The ordinary least-squares performs as a robust all-round fitting method. For the other methods such as weighted least-squares and maximum likelihood-estimation there are implementation choices that have to be made carefully, or the methods will result in a higher bias or outliers. Using correctly regularized and bootstrapped weighted least-squares and maximum likelihood-estimation can result in better variance of the estimate, but the difference is small for a higher number of data points or a high number of shots.

The model violation score is a useful tool for adding a quality estimate to fitted data.

## 5 Acknowledgements

This work was supported by the Dutch National Growth Fund (NGF), as part of the Quantum Delta NL programme and by the European Union's Horizon 2020 research and innovation programme under the Grant Agreement No.951852 (QLSI project).

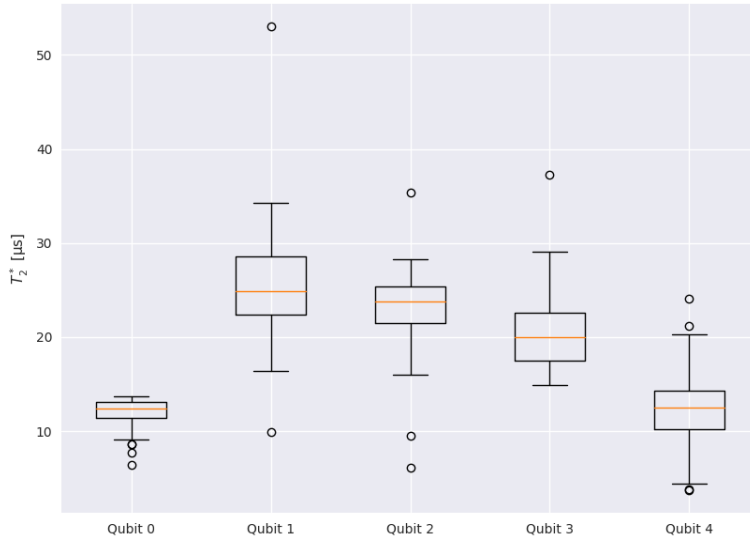


Figure 11:  $T_2^*$  values for measurements on Starmon-5

## References

- [1] Qiskit contributors. Probability — Qiskit Experiments 0.4.0 documentation.
- [2] Fabian Dablander. Two perspectives on regularization — Fabian Dablander.
- [3] Martin A. Fischler and Robert C. Bolles. Random sample consensus: A paradigm for model fitting with applications to image analysis and automated cartography. In Martin A. Fischler and Oscar Firschein, editors, *Readings in Computer Vision*, pages 726–740. Morgan Kaufmann, San Francisco (CA), 1987.
- [4] Henri P. Gavin. The levenberg-marquardt method for nonlinear least squares curve-fitting problems c ©. 2013.
- [5] Gregory Gundersen. Asymptotic Normality of Maximum Likelihood Estimators.
- [6] Richard Hartley and Andrew Zisserman. *Multiple View Geometry in Computer Vision*. Cambridge University Press, New York, NY, USA, 2 edition, 2003.
- [7] Thorsten Last, Nodar Samkharadze, Pieter Eendebak, Richard Versluis, Xiao Xue, Amir Sammak, Delphine Brousse, Kelvin Loh, Henk Polinder, Giordano Scappucci, Menno Veldhorst, Lieven Vandersypen, Klara Maturova, Jeremy Veltin, and Garrelt Alberts. Quantum Inspire: QuTech’s platform for co-development and collaboration in quantum computing. In Eric M. Panning and Martha I. Sanchez, editors, *Novel Patterning Technologies for Semiconductors, MEMS/NEMS and MOEMS 2020*, volume 11324, page 17. SPIE-Intl Soc Optical Eng, mar 2020.
- [8] Donald W. Marquardt. An algorithm for least-squares estimation of nonlinear parameters. *Journal of the Society for Industrial and Applied Mathematics*, 11(2):431–441, 1963.
- [9] Matt Newville, Renee Otten, Andrew Nelson, Antonino Ingargiola, Till Stensitzki, Dan Allan, Austin Fox, Faustin Carter, Michał, Ray Osborn, Dima Pustakhod, Ineuhaus, Sebastian Weigand, Glenn, Christoph Deil, Mark, Allan L. R. Hansen, Gustavo Pasquevich, Leon Foks, Nicholas Zobrist, Oliver Frost, Alexandre Beelen, Stuermer, azelcer, Andrew Hannum, Anthony Polloreno, Jens Hedegaard Nielsen, Shane Caldwell, Anthony Almarza, and Arun Persaud. lmfit/lmfit-py: 1.0.3, October 2021.
- [10] Erik Nielsen, John King Gamble, Kenneth Rudinger, Travis Scholten, Kevin Young, and Robin Blume-Kohout. Gate Set Tomography. *Quantum*, 5:557, October 2021.

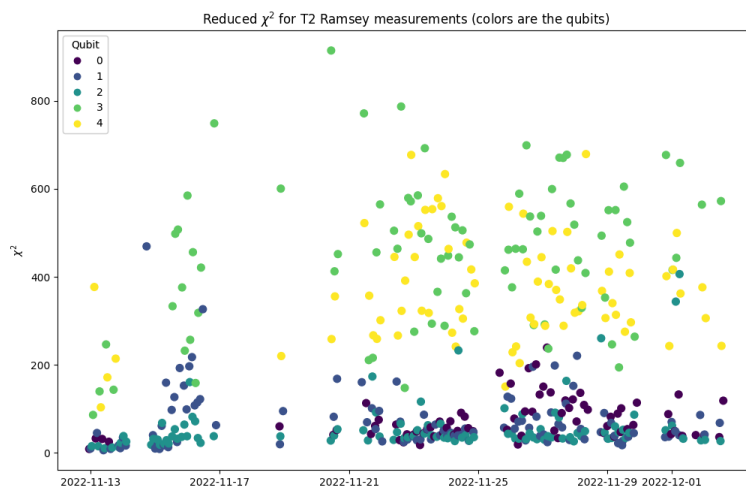


Figure 12:  $\chi^2$  values for  $T_2^*$  measurements on Starmon-5

- [11] Michael A. Nielsen and Isaac L. Chuang. *Quantum computation and quantum information*. Cambridge University Press, 2000.
- [12] Stephan G. J. Philips, Mateusz T. Mądzik, Sergey V. Amitonov, Sander L. de Snoo, Maximilian Russ, Nima Kalhor, Christian Volk, William I. L. Lawrie, Delphine Brousse, Larysa Tryputen, Brian Paquelet Wuetz, Amir Sammak, Menno Veldhorst, Giordano Scappucci, and Lieven M. K. Vandersypen. Universal control of a six-qubit quantum processor in silicon. *Nature*, feb 2022.
- [13] J. P.G. Van Dijk, E. Kawakami, R. N. Schouten, M. Veldhorst, L. M.K. Vandersypen, M. Babaie, E. Charbon, and F. Sebastiano. Impact of Classical Control Electronics on Qubit Fidelity. *Physical Review Applied*, 12(4):44054, oct 2019.
- [14] Wikipedia contributors. Bias–variance tradeoff — Wikipedia, the free encyclopedia. [https://en.wikipedia.org/w/index.php?title=Bias%E2%80%93variance\\_tradeoff&oldid=1121715949](https://en.wikipedia.org/w/index.php?title=Bias%E2%80%93variance_tradeoff&oldid=1121715949), 2022. [Online; accessed 25-November-2022].
- [15] Wikipedia contributors. Bootstrapping (statistics) — Wikipedia, the free encyclopedia. [https://en.wikipedia.org/w/index.php?title=Bootstrapping\\_\(statistics\)&oldid=1119697347](https://en.wikipedia.org/w/index.php?title=Bootstrapping_(statistics)&oldid=1119697347), 2022. [Online; accessed 6-December-2022].
- [16] Wikipedia contributors. Gauss–markov theorem — Wikipedia, the free encyclopedia. Gauss–Markov theorem — Wikipedia, 2022. [Online; accessed 28-November-2022].
- [17] Wikipedia contributors. Non-linear least squares — Wikipedia, the free encyclopedia. [https://en.wikipedia.org/w/index.php?title=Non-linear\\_least\\_squares&oldid=1103186857](https://en.wikipedia.org/w/index.php?title=Non-linear_least_squares&oldid=1103186857), 2022. [Online; accessed 28-November-2022].
- [18] Wikipedia contributors. Binomial proportion confidence interval — Wikipedia, the free encyclopedia, 2025. [Online; accessed 17-February-2025].



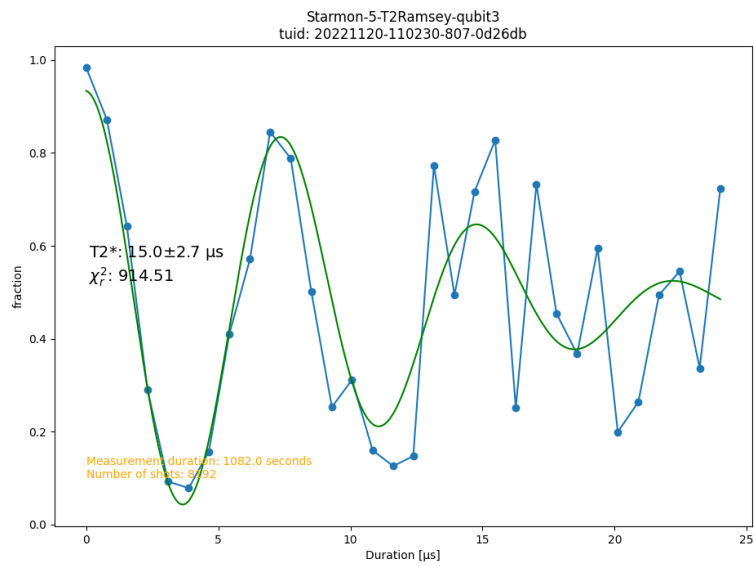


Figure 13:  $T_2^*$  measurement on Starmon-5. The data points for small waiting time are good, for large waiting time the data seems non-coherent. The estimated value for  $T_2^*$  itself is very reasonable, but the model violation  $\chi_r^2$  is very high. Blue: measured data points, green: fitted model.

## A Results for fitting an exponential model

In this section we show results for fitting an exponential model  $F(x, p) = p_0 + p_1 \exp(-p_2 x)$  with parameters  $p = (\text{offset}, \text{scale}, \gamma)$ . The model and generated data points are shown in figure 14. All methods are identical to the methods for the results of the sine model described in section 3. In figure 15, figure 16 and figure 17 the distributions for the  $\gamma$ , scale and offset parameters are shown. The results for the various fitting methods are comparable to the sine fitting results.

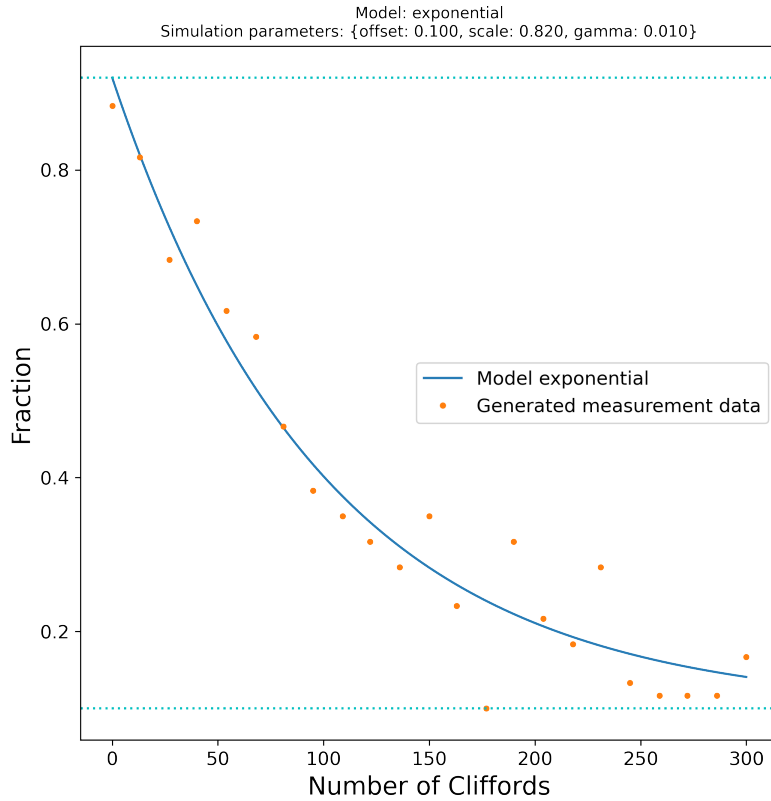


Figure 14: Model for exponential with simulated data

### A.1 Maximum-likelihood fitting without penalty term

For the exponential model we compare the ordinary least-squares and maximum likelihood-estimation with various penalty terms. The distribution of the  $\gamma$  parameter is in figure 18. It is clear that without a penalty term there is a strong bias in the result. The soft and hard penalty have comparable results.

## B Variance estimation details

From a measured fraction we can estimate a variance in the datapoint. Different options are shown in figure 19.

Model exponential, parameter gamma, N 23, number of shots 60,  
simulation parameters 'offset': 0.1, 'scale': 0.82, 'gamma': 0.01

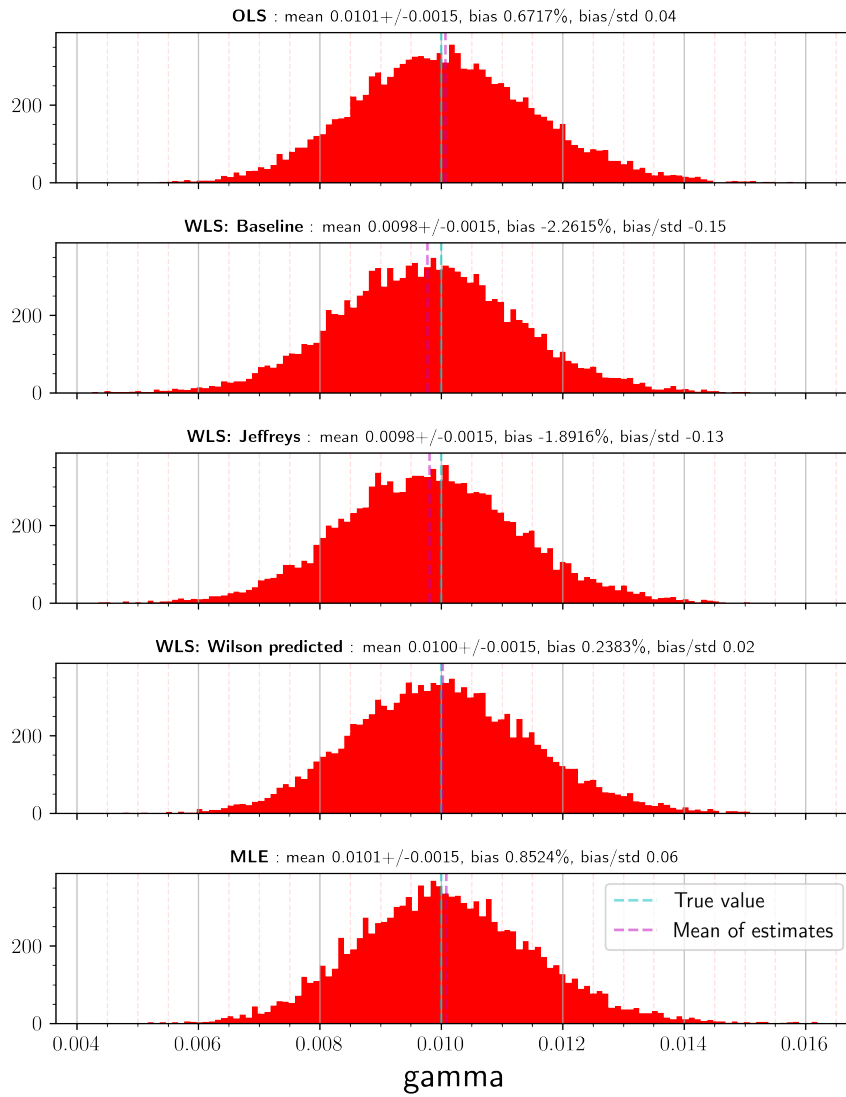


Figure 15: Distribution of the gamma parameter for an exponential model

Model exponential, parameter scale, N 23, number of shots 60,  
simulation parameters 'offset': 0.1, 'scale': 0.82, 'gamma': 0.01

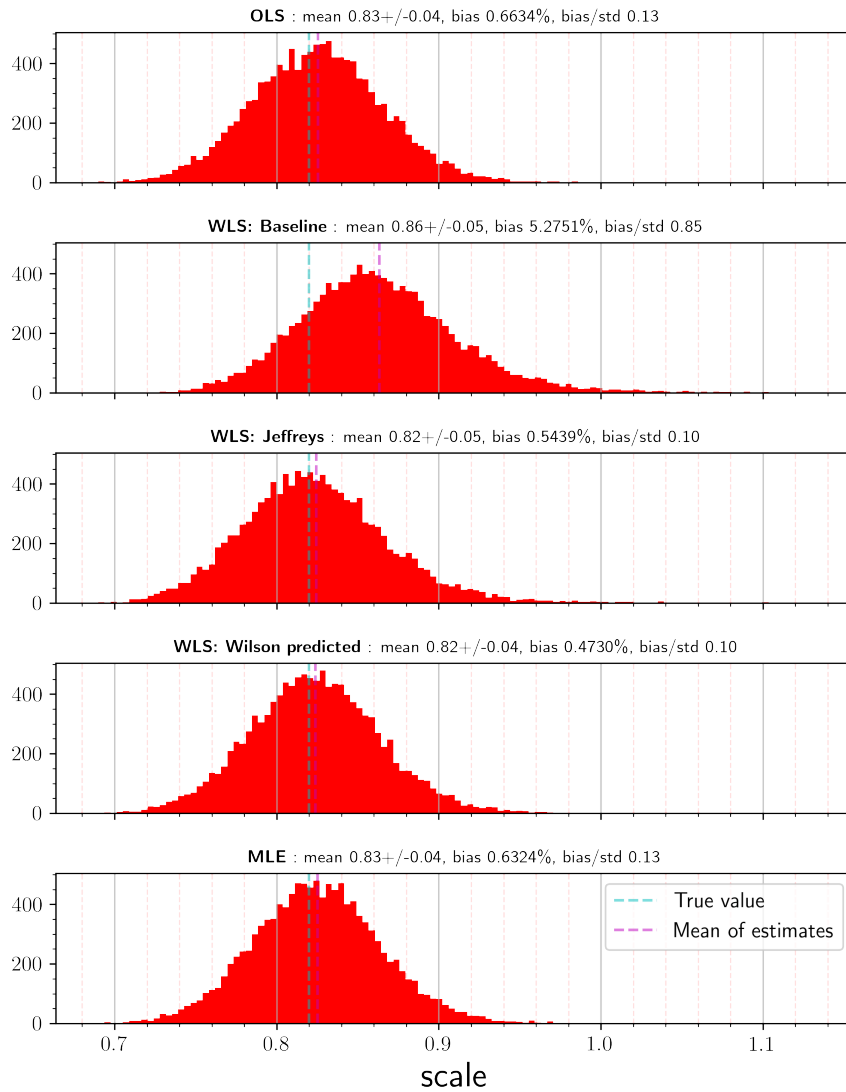


Figure 16: Distribution of the `scale` parameter for an exponential model

Model exponential, parameter offset, N 23, number of shots 60,  
simulation parameters 'offset': 0.1, 'scale': 0.82, 'gamma': 0.01

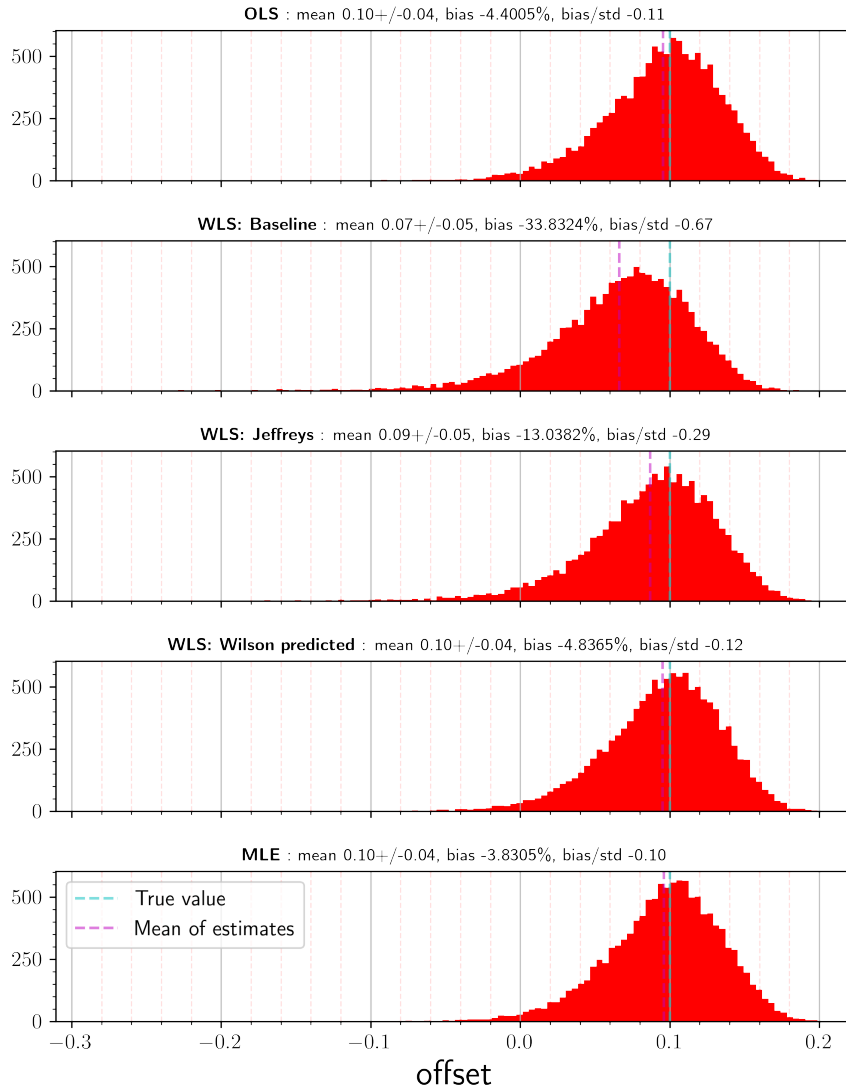


Figure 17: Distribution of the **offset** parameter for an exponential model

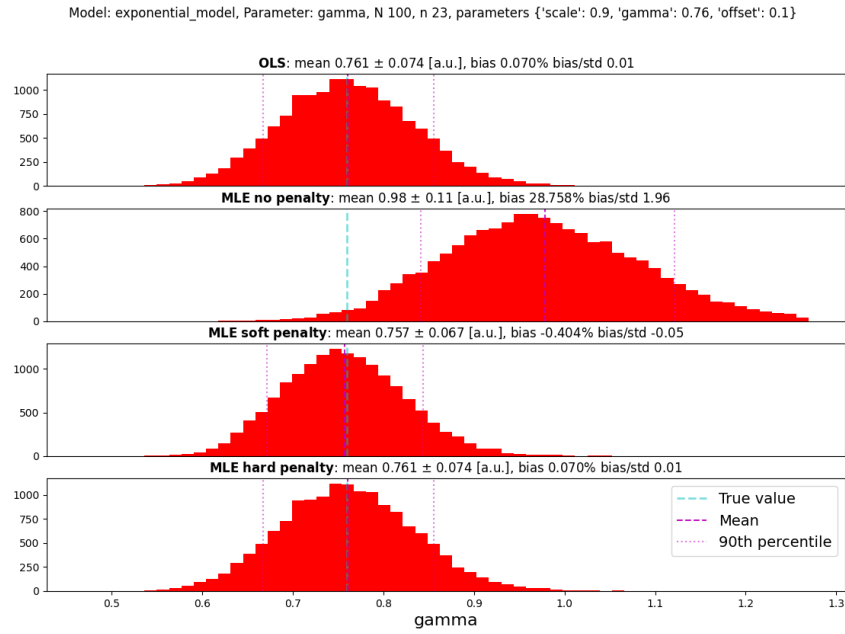


Figure 18: Distribution of the gamma parameter for an exponential model

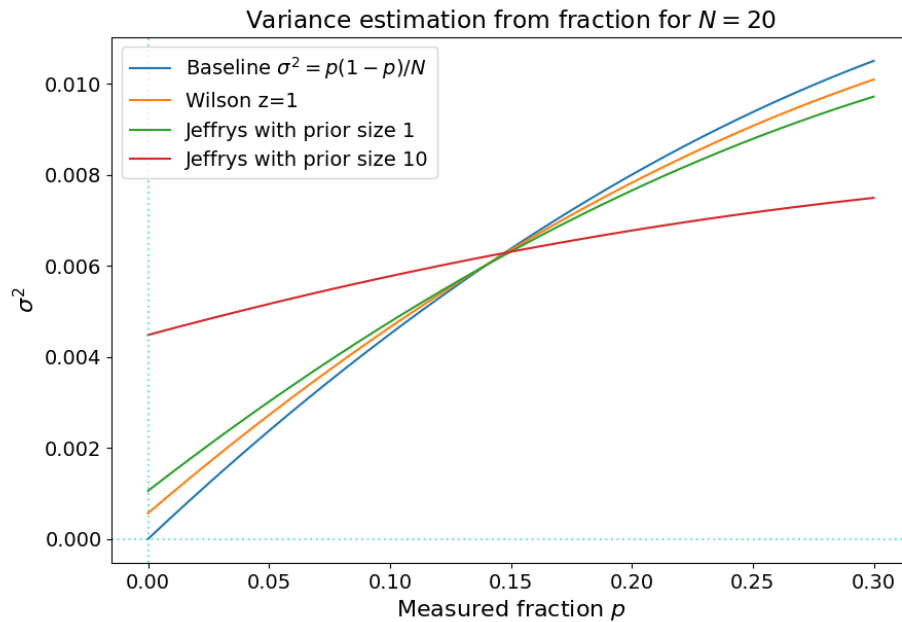


Figure 19: Different estimators for the variance from a measured fraction